

the original frequency again. More detailed analysis of the data revealed additional weak speckles earlier in the original 6-UT hour, at about 06:20 UT, when the transmitter was operated at a lower frequency (and lower effective power), and some of the brightest speckles were also identified in data from one of the other lower-resolution camera systems operated from a separate building, eliminating any doubt that the speckles represent actual light from the sky.

Although visible levels of artificial optical emissions have not been reported previously, there have been other attempts made to stimulate the auroral E layer with radio waves. A similar experiment that used low-light television cameras and a 2-s on-off cycle but different polarization reported an estimated modulation of less than 10 R, interpreted as radio-induced decreases in the green line emission⁷. Large-scale structural changes in the overhead aurora have been reported in conjunction with E-layer heating⁸, but the extremely small number of cases and the close similarity of the observed effects to naturally occurring processes make it difficult to assess the true influence of the radio waves on the auroral events. In contrast, the recent HAARP observations demonstrate clear on-off control of the speckles over 50 or more complete cycles.

Potential sources of the observed bright speckles fall into two categories: production in the local E-region ionosphere by the transmitter beam, or indirect creation by modification of the auroral particle precipitation, which then produces the optical speckles in the same way as the background aurora. If the speckles are locally generated, the role of the natural aurora would probably be limited to creation of the E layer for the radio waves to interact with, and it might be possible to generate similar phenomena in non-auroral E layers independent of any specific on-off cycling, a potentially desirable condition for creation of visible artificial light. If, on the other hand, the speckles result from modification of the auroral particle population, perhaps through perturbations to currents flowing in the E layer or a wave resonance, we expect that the specific frequency of the on-off cycling relative to the natural pulsation frequencies might be a critical parameter, and experiments of this type could potentially become a new tool for exploration of time-dependent processes in the aurora and magnetosphere. □

Received 13 September; accepted 6 December 2004; doi:10.1038/nature03243.

1. Bailey, V. A. On some effects caused in the ionosphere by electric waves, Part II. *Phil. Mag.* **26**(7), 425–453 (1938).
2. Bernhardt, P., Duncan, L. M. & Tepley, C. A. Artificial airglow excited by high-power radio waves. *Science* **242**, 1022–1027 (1988).
3. Chamberlain, J. W. *Physics of the Aurora and Airglow* (International Geophysics Series Vol. 2, Academic, New York, 1961).
4. Rishbeth, H. & Garriot, O. K. *Introduction to Ionospheric Physics* (Academic, New York, 1969).
5. Djuth, F. T. et al. Large airglow enhancements produced via wave-plasma interactions in sporadic E. *Geophys. Res. Lett.* **26**, 1557–1560 (1999).
6. Omholt, A. *The Optical Aurora 6* (Physics and Chemistry in Space Vol. 4, Springer, New York, 1971).
7. Sergienko, T., Kornilov, I., Belova, E., Turunen, T. & Manninen, J. Optical effects in the aurora caused by ionospheric HF heating. *J. Atmos. Sol-Terr. Phys.* **59**, 2401–2407 (1997).
8. Blagoveshchenskaya, N. F. et al. Ionospheric HF pump wave triggering of local auroral activation. *J. Geophys. Res.* **106**, 29071–29089 (2001).
9. Bauer, S. J. *Physics of Planetary Ionospheres 82–95* (Physics and Chemistry in Space Vol. 6, Springer, New York, 1973).
10. Davis, N. *The Aurora Watchers Handbook 58* (Univ. Alaska Press, Fairbanks, 1992).
11. Carlson, H. C. Jr & Egeland, A. in *Introduction to Space Physics* (eds Kivelson, M. G. & Russell, V.) 459–502 (Cambridge Press, New York, 1995).

Acknowledgements HAARP is a Department of Defense programme operated jointly by the US Air Force and US Navy. We thank E. Mishin for his contributions to the experiment planning and P. Ning for operating the all-sky imager.

Competing interests statement The authors declare that they have no competing financial interests.

Correspondence and requests for materials should be addressed to T.R.P. (todd.pedersen@hanscom.af.mil).

Observation of random-phase lattice solitons

Oren Cohen¹, Guy Bartal¹, Hrvoje Buljan^{1,2}, Tal Carmon¹, Jason W. Fleischer^{1,3}, Mordechai Segev^{1,3} & Demetrios N. Christodoulides⁴

¹Physics Department and Solid State Institute, Technion – Israel Institute of Technology, Haifa 32000, Israel

²Department of Physics, University of Zagreb, PP331, 10000 Zagreb, Croatia

³Electrical Engineering Department, Princeton University, Princeton, New Jersey 08544, USA

⁴School of Optics/CREOL, University of Central Florida, Florida 32816-2700, USA

The coherence of waves in periodic systems (lattices) is crucial to their dynamics, as interference effects, such as Bragg reflections, largely determine their propagation. Whereas linear systems allow superposition, nonlinearity introduces a non-trivial interplay between localization effects, coupling between lattice sites, and incoherence. Until recently, all research on solitary waves (solitons) in nonlinear lattices has involved only coherent waves. In such cases, linear dispersion or diffraction of wave packets can be balanced by nonlinear effects, resulting in coherent lattice (or ‘discrete’) solitons^{1,2}; these have been studied in many branches of science^{3–11}. However, in most natural systems, waves with only partial coherence are more common, because fluctuations (thermal, quantum or some other) can reduce the correlation length to a distance comparable to the lattice spacing. Such systems should support random-phase lattice solitons displaying distinct features¹². Here we report the experimental observation of random-phase lattice solitons, demonstrating their self-trapping and local periodicity in real space, in addition to their multi-peaked power spectrum in momentum space. We discuss the relevance of such solitons to other nonlinear periodic systems in which fluctuating waves propagate, such as atomic systems, plasmas and molecular chains.

Wave propagation in periodic potentials exhibits universal characteristic features, such as Bragg reflections, bandgaps (stop bands) and alternating regions of normal and anomalous dispersion. In solid-state physics, this leads to regions where the effective mass is positive or negative¹³, whereas in optical settings such as waveguide arrays¹ the same processes correspond to regimes of normal/anomalous diffraction. These effects all result from interference among waves propagating in the lattice, and as such they critically depend on the degree of coherence of the waves involved. The propagation dynamics of incoherent waves in nonlinear periodic potentials depend on the threefold interplay between interference effects, nonlinearity and the statistical (coherence) properties of the waves. As a result, many fundamental physical phenomena occurring with coherent waves, such as solitons^{1–10}, modulation instability^{6,14} and Bloch oscillations^{15,16}, are expected to exhibit new features with incoherent (random-phase) waves. Likewise, potential applications will offer new possibilities when partial coherence plays a role and is used as an additional degree of freedom. For example, using random-phase waves as a statistical probe may provide a valuable tool for exploring general dynamics in nonlinear lattices¹⁷. Another example is the extension of our current experimental findings to obtain Brillouin zone spectroscopy. To date, the only work in this direction has been the theoretical prediction of one-dimensional random-phase lattice solitons (RPLSs)¹². We report the experimental observation of incoherent optical lattice solitons in a nonlinear waveguide array.

Before discussing the new features introduced by the partial coherence of waves, we will highlight the most relevant physical

processes associated with the lattice. As periodicity and Bragg reflections dominate the linear properties, and as the spatial power spectrum characterizes the probe beam, it is best to consider the lattice properties through its k -space (momentum space) representation. Figure 1a shows the first and second Brillouin zones of a two-dimensional square lattice with the high-symmetry points (Γ , X and M) marked with white dots. The first two bands in the transmission spectrum are shown in Fig. 1b, and the dispersion curves between the symmetry points of the first two bands are plotted in Fig. 1c. Negative curvature in these figures corresponds to normal diffraction; that is, a narrow beam with its power spectrum centred in a normal diffraction region acquires a convex phase front during linear propagation, in a fashion similar to diffraction in homogeneous media. On the other hand, positive curvature in the dispersion relation corresponds to regions of anomalous diffraction, in which a beam (wave packet) acquires a concave phase front while propagating linearly. A self-focusing nonlinearity can only counteract the broadening tendency of a narrow beam experiencing normal diffraction. Hence, a bright soliton in a self-focusing nonlinear photonic lattice should significantly populate those regions in k -space where the diffraction is normal. Consequently, the power spectrum of random-phase lattice solitons in self-focusing media is expected to have multiple humps, with the humps located in regions of negative (normal) curvature¹². Specifically, for a self-focusing, square, nonlinear photonic lattice, Fig. 1b and c indicates that the power spectrum of a two-band RPLS should consist of a central hump centred on the Γ -point of the first band together with four humps centred on the vicinity of the X-points of the second band.

Our experiments were carried out in optically induced nonlinear photonic lattices¹⁸, recently used for the experimental observations of two-dimensional lattice solitons¹⁹, spatial gap solitons^{19,20}, vortex lattice solitons^{21,22}, dipole-mode discrete solitons²³ and 'optical polarons'²⁴. In this system, plane waves interfering in a photorefractive crystal induce a photonic lattice (Fig. 1d), while voltage applied across the crystal controls the strength of the photorefractive screening nonlinearity^{25,26}. We photograph the light leaving the

output face of the crystal both in real space and in k -space (for the latter we use a lens, and monitor the intensity at the focal plane). A quasi-thermal (partially spatially coherent) quasi-monochromatic source is established by focusing a laser beam onto a rotating diffuser^{27,28}, and then imaging 1:1 with a telescopic (so-called '4f') imaging system onto the input face of the crystal (Fig. 1e). We control the degree of spatial coherence and the power spectrum of the exciting beam by a spatial filter in the Fourier plane of the 4f system. Finally, we note that the nonlinear response time of the medium is much longer than the fluctuation time of the incoherent beam; hence, it can support incoherent solitons^{27,29}.

Figure 2a shows a real-space photograph of the induced square lattice and of a probe beam launched into the lattice, at the input face of the crystal. The lattice period is $\sim 11.5 \mu\text{m}$, and the probe beam has a width of $26 \mu\text{m}$ (full-width at half-maximum, FWHM). Hence, the probe beam covers an area of several (~ 10 – 12) channels. Figure 2b shows the Fourier power spectrum when the probe beam is incoherent (wide blue circle) and of the lattice-forming waves (four dots; 'delta functions'). Because the inducing array beams form Bragg angles in our system, the corresponding square defined by the four dots outlines the first Brillouin zone (Fig. 1a). The wide, blue circle shows that the power spectrum of the incoherent probe beam covers all the first Brillouin zone and significant parts of the second zone. For comparison, Fig. 2c shows the power spectrum of a coherent probe beam (with the diffuser removed) possessing the same size (envelope) in real space as the incoherent probe. The spectral width of such a coherent probe beam is much less than that of the incoherent probe (by a factor greater than 3), and covers only a small portion of the first Brillouin zone. Going back to Fig. 2b, the width indicates that the average speckle size in the incoherent beam is less than one-third the size of the envelope of the beam, and that the spatial correlation distance of this random-phase beam is approximately equal to the lattice period.

The incoherent beam is focused into the lattice with the real-space distribution and power spectrum shown in Fig. 2a and b, respectively, and propagates through a 5-mm nonlinear photonic

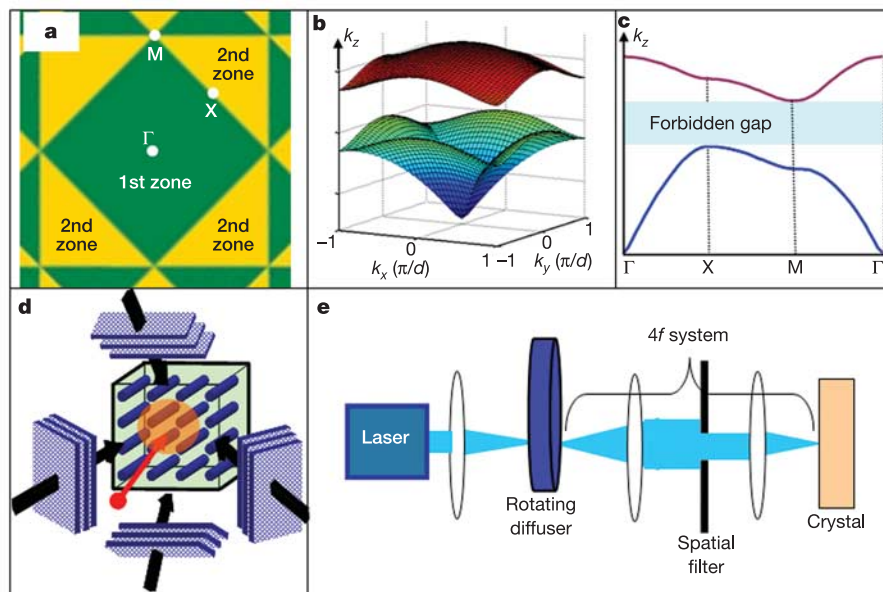


Figure 1 Experimental scheme for producing random-phase solitons in an optically induced square lattice. **a**, First (green square) and second (four yellow triangles) Brillouin zones of a two-dimensional square lattice with the high-symmetry points (Γ , X and M) marked with white dots. **b**, Transmission spectrum of the first two bands of a two-dimensional square lattice with a lattice period d . **c**, Dispersion curves between the symmetry points of the first two bands. Negative curvature in these curves corresponds to

normal diffraction regions. **d**, Diagram of the optical induction technique used to obtain the two-dimensional, square photonic lattice. The blue planes with heavy black arrows indicate the plane waves used to optically induce the lattice. The red arrow indicates the direction of a probe beam entering the lattice. The orange circle indicates the width of the probe beam. **e**, Diagram of our set-up for obtaining a spatially incoherent (quasi-thermal), quasi-monochromatic beam.

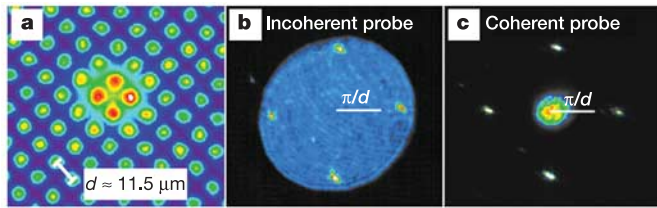


Figure 2 Experimental images at the input face. **a**, Real-space picture of the induced square lattice (with lattice period d) and a probe beam. **b**, Power spectrum of the incoherent probe beam (blue circle) and lattice beams (four dots), which define the corners of the first Brillouin zone. The power spectrum resides in the first and second Brillouin zones. **c**, Same as **b** but with a coherent probe beam that has the same size in real space (as in **a**).

lattice. As in ref. 19, each array beam has ~ 15 mW of power, while the nonlinearity is set by applying 1 kV across the crystal. Typical experimental pictures taken at the output face are shown in Fig. 3. Figure 3a shows linear diffraction for a low-intensity probe beam, characterized by a 1:50 intensity ratio between the probe and array beams. Note that the diffracted output is roughly 2.5 times the input width of the probe. At $10\times$ higher intensity (1:5 ratio), the incoherent probe beam self-traps and forms an RPLS. Figure 3b shows an RPLS centred on a lattice site (a waveguide), while Fig. 3c and d shows RPLSs centred between 2 lattice sites and 4 lattice sites, respectively. Figure 3e depicts the power spectrum of the RPLSs. As before, the four dots represent the array beams, defining the M-symmetry points at the corners of the first Brillouin zone. The power spectrum of the solitons takes on the square symmetry of the lattice and is clearly multi-humped, with well-separated peaks located in the normal diffraction regions of the first two Brillouin zones. For comparison, we monitor the linear and nonlinear propagation of the probe beam with the index lattice removed (that is, in a homogeneous medium). To do this, we block the lattice beams, while maintaining all the other experimental parameters (applied bias field and intensity). We observe that the beam undergoes self-focusing, yet the nonlinearity is too weak to fully balance the linear diffraction broadening of the beam, and thus cannot form an incoherent soliton. Figure 3f shows the power spectrum of the output probe beam. In a sharp contrast to the RPLS spectrum, the self-focused, incoherent beam propagating in the homogeneous (no lattice) nonlinear crystal retains its homogeneity, exhibiting no multi-hump structure.

Next we study the formation of an RPLS with a beam that is more coherent than that of Fig. 3, under similar self-focusing conditions. Figure 4a and b shows respectively the real-space photograph and the power spectrum of the beam, at the input face of the crystal. In this case, the input power spectrum covers (approximately) the first

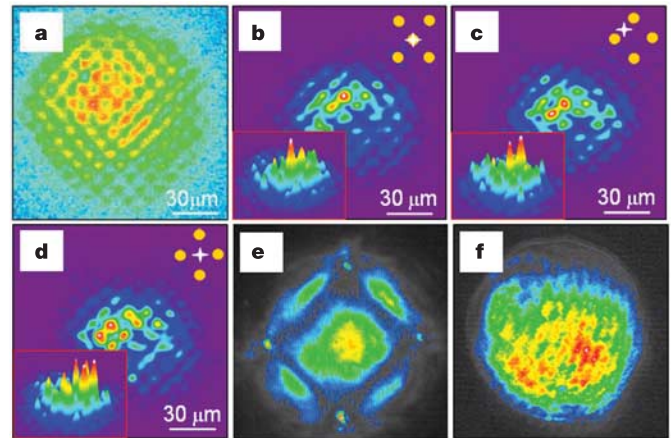


Figure 3 Experimental images at the output face. **a**, Linear lattice diffraction of the incoherent beam. **b–d**, Real-space pictures of random-phase lattice solitons (RPLSs) centred on a site (**b**), between two sites (**c**), and between four sites (**d**). The insets show three-dimensional perspectives of the solitons. Note that **a–d** have the same scale, and the linearly diffracted beam of **a** is at least 2.5 times the width of the soliton. **e**, Power spectrum of an RPLS, displaying its square symmetry and multi-humped structure with the peaks located in the normal diffraction regions of the first two bands. The four dots correspond to the power spectrum of the array beams. **f**, Power spectrum of the self-focused incoherent probe beam at the output face of the crystal without the lattice. Red (blue) colour indicates high (low) intensity.

Brillouin zone only. Figure 4c shows linear diffraction in the lattice for a low-intensity probe beam, while Fig. 4d shows the RPLS when the beam intensity is sufficiently increased. As a consequence of the increased coherence, the linear broadening of the beam is smaller and the formed RPLS is tighter (relative to Fig. 3b). Finally, Fig. 4e depicts the power spectrum of the RPLS. Interestingly, this spectrum is also multi-humped, populating the normal diffraction parts of the first and the second (initially unexcited) Brillouin zones. That is, the input beam with a power spectrum in the first band only reshapes into the RPLS, and in doing so transfers part of the power to the normal diffraction region of the second band while leaving the anomalous diffraction region of the first band unpopulated.

We note that originally, while planning these experiments, we believed that we would have to ‘engineer’ the power spectrum of the initial probe beam to match the multi-humped k -distribution of the RPLS¹². Unexpectedly, we found experimentally that a probe beam with a homogeneous k -space distribution (a single hump with a proper width) self-adjusts its spectrum and evolves naturally, under proper nonlinear conditions, into an RPLS. This cannot be seen using real-space imaging, but the Fourier imaging technique

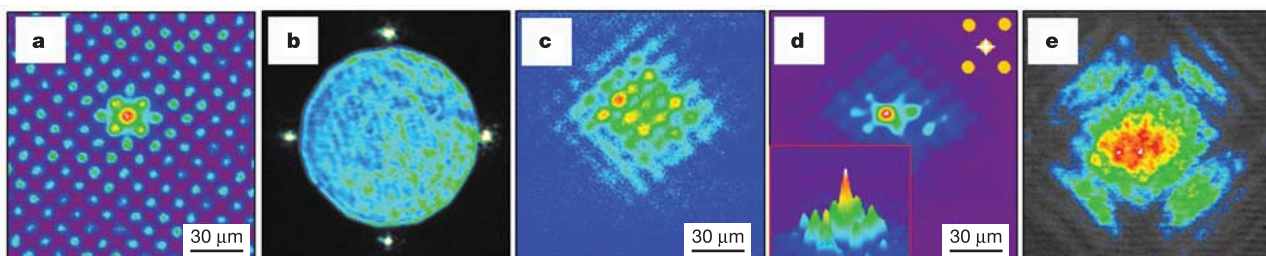


Figure 4 An RPLS with a lower incoherence than the RPLS of Figs 2 and 3. **a**, Real-space photograph of induced square lattice and the probe beam. **b**, Power spectrum of the incoherent input probe beam (blue circle) and lattice beams (four dots); the input spectrum

resides in the first band only. **c**, Linear lattice diffraction of the incoherent beam. **d, e**, Real-space image (**d**) and power spectrum (**e**) of the emerging RPLS under proper self-focusing conditions.

presented here clearly shows the difference between the simple spectrum of the input (Fig. 2b) and the complex multi-hump spectrum of the output (Fig. 3e). During propagation, then, there is a **k**-space evolution in which energy transfers from regions of anomalous diffraction to regions of normal diffraction. Moreover, Fig. 4b and e clearly shows that energy transfers between bands. Because different **k**-vectors correspond to different Bloch modes, this energy transfer corresponds to an inherently nonlinear coupling between modes of the linear lattice. In this sense, our measurements are related to the Fermi–Pasta–Ulam problem³⁰. In the Fermi–Pasta–Ulam system, a lattice mode was excited, and it was expected that nonlinearity would redistribute the energy to a homogeneous state, that is, lead to equipartition. Instead, energy recurred to the initial mode, exhibiting energy oscillations between the initial mode and a finite group of modes, in an almost periodic fashion. In our system, an initially homogeneous **k**-space distribution evolves into a steady-state multi-humped soliton power spectrum. The focus of this Letter has been on the observation of these RPLs, but the rich dynamics underlying this energy transfer suggests many applications. For example, the spatially incoherent input beam can be used as a probe with given statistics, and the imaging techniques outlined here allow the observation of nonlinear effects, in both real and Fourier space.

Our experiments open up new possibilities in other nonlinear periodic systems beyond optics. For example, one can think of random-phase matter-wave lattice solitons in Bose–Einstein condensates, where the periodic potential is also optically induced. Similarly, one can envision random-phase solitons occurring with vibrational waves propagating along periodic molecular structures, finite-temperature plasma waves, or with charge-density waves in polymers or in crystalline conductors. In a more general sense, RPLs should exist in any nonlinear periodic system, because fluctuations (quantum, thermal, and so on) are always present and the propagating waves are never fully correlated. □

Received 24 June; accepted 10 December 2004; doi:10.1038/nature03267.

1. Christodoulides, D. N., Lederer, F. & Silberberg, Y. Discretizing light behaviour in linear and nonlinear waveguide lattices. *Nature* **424**, 817–823 (2003).
2. Campbell, D. K., Flach, S. & Kivshar, Yu. S. Localizing energy through nonlinearity and discreteness. *Phys. Today* **57**(1), 43–49 (Jan. 2004).
3. Daydov, A. S. & Kislukha, N. I. Solitary excitation in one-dimensional molecular chains. *Phys. Status Solidi B* **59**, 465–470 (1973).
4. Xie, A., van der Meer, L., Hoff, W. & Austin, R. H. Long-lived amide I vibrational modes in myoglobin. *Phys. Rev. Lett.* **84**, 5435–5438 (2000).
5. Su, W. P., Schieffer, J. R. & Heeger, A. J. Solitons in polyacetylene. *Phys. Rev. Lett.* **42**, 1698–1701 (1979).
6. Christodoulides, D. N. & Joseph, R. I. Discrete self focusing in nonlinear arrays of coupled waveguides. *Opt. Lett.* **13**, 794–796 (1988).
7. Eisenberg, H. S., Silberberg, Y., Morandotti, R., Boyd, A. R. & Aitchinson, J. S. Discrete spatial optical solitons in waveguide arrays. *Phys. Rev. Lett.* **81**, 3383–3386 (1998).
8. Sievers, A. J. & Takeno, S. Intrinsic localized modes in anharmonic crystal. *Phys. Rev. Lett.* **61**, 970–973 (1988).
9. Schwartz, U. T., English, L. Q. & Sievers, A. J. Experimental generation and observation of intrinsic localized spin wave modes in an antiferromagnet. *Phys. Rev. Lett.* **83**, 223–226 (1999).
10. Trombettoni, A. & Smerzi, A. Discrete solitons and breathers with dilute Bose–Einstein condensate. *Phys. Rev. Lett.* **86**, 2353–2356 (2001).
11. Eiermann, B. *et al.* Bright Bose–Einstein gap solitons of atoms with repulsive interaction. *Phys. Rev. Lett.* **92**, 230401 (2004).
12. Buljan, H. *et al.* Random phase solitons in nonlinear periodic lattices. *Phys. Rev. Lett.* **92**, 223901 (2004).
13. Ashcroft, N. W. & Mermin, N. D. *Solid State Physics* (Saunders, Philadelphia, 1976).
14. Meier, J. *et al.* Experimental observation of discrete modulation instability. *Phys. Rev. Lett.* **92**, 163902 (2004).
15. Pertsch, T., Dannberg, P., Elflein, W., Brauer, A. & Lederer, F. Optical Bloch oscillations in temperature tuned waveguide arrays. *Phys. Rev. Lett.* **83**, 4752–4755 (1999).
16. Morandotti, R., Peschel, U., Aitchison, J. S., Eisenberg, H. S. & Silberberg, Y. Experimental observation of linear and nonlinear optical Bloch oscillations. *Phys. Rev. Lett.* **83**, 4756–4759 (1999).
17. Frisch, U. *Turbulence* (Cambridge Univ. Press, Cambridge, UK, 1995).
18. Efremidis, N. K., Sears, S., Christodoulides, D. N., Fleischer, J. W. & Segev, M. Discrete solitons in photorefractive optically induced photonic lattices. *Phys. Rev. E* **66**, 046602 (2002).
19. Fleischer, J. W., Segev, M., Efremidis, N. K. & Christodoulides, D. N. Observation of two-dimensional discrete solitons in optically induced nonlinear photonic lattices. *Nature* **422**, 147–150 (2003).
20. Fleischer, J. W., Carmon, T., Segev, M., Efremidis, N. K. & Christodoulides, D. N. Observation of discrete solitons in optically induced real time waveguide arrays. *Phys. Rev. Lett.* **90**, 023902 (2003).

21. Fleischer, J. W. *et al.* Observation of vortex ring “discrete” solitons in 2D photonic lattices. *Phys. Rev. Lett.* **92**, 123904 (2004).
22. Neshev, D. N. *et al.* Observation of discrete vortex solitons in optically-induced photonic lattices. *Phys. Rev. Lett.* **92**, 123903 (2004).
23. Neshev, D., Ostrovskaya, E., Kivshar, Yu. S. & Krokolkowski, W. Spatial solitons in optically induced gratings. *Opt. Lett.* **28**, 710–712 (2003).
24. Martin, H., Eugenieva, E. D., Chen, Z. G. & Christodoulides, D. N. Discrete solitons and soliton-induced dislocations in partially coherent photonic lattices. *Phys. Rev. Lett.* **92**, 123902 (2004).
25. Segev, M., Valley, G. C., Crosignani, B., Diperto, P. & Yariv, A. Steady state spatial screening-soliton in photorefractive media with external applied field. *Phys. Rev. Lett.* **73**, 3211–3214 (1994).
26. Christodoulides, D. N. & Carvalho, M. I. Bright, dark and gray spatial soliton states in photorefractive media. *J. Opt. Soc. Am. B* **12**, 1628–1633 (1995).
27. Mitchell, M., Chen, Z., Shih, M. & Segev, M. Self-trapping of partially spatially-incoherent light. *Phys. Rev. Lett.* **77**, 490–493 (1996).
28. Goodman, J. *Statistical Optics* (Wiley & Sons, New York, 1985).
29. Mitchell, M. & Segev, M. Self-trapping of incoherent white light. *Nature* **387**, 880–883 (1997).
30. Fermi, E., Pasta, J. & Ulam, S. Report LA-1940 (LANL, Los Alamos, 1955).

Acknowledgements This work was supported by the Israeli Science Foundation, the Israel–USA Binational Science Foundation, and by the German–Israeli DIP Project. O.C. acknowledges the generous support of the Israeli Ministry of Science through the Eshkol Fellowship.

Competing interests statement The authors declare that they have no competing financial interests.

Correspondence and requests for materials should be addressed to M.S. (msegev@tx.technion.ac.il).

Conversion of large-amplitude vibration to electron excitation at a metal surface

Jason D. White¹, Jun Chen¹, Daniel Matsiev¹, Daniel J. Auerbach² & Alec M. Wodtke¹

¹Department of Chemistry and Biochemistry, University of California, Santa Barbara, California 93106, USA

²Hitachi Global Storage Technologies, 650 Harry Road, San Jose, California 95120-6099, USA

Gaining insight into the nature and dynamics of the transition state is the essence of mechanistic investigations of chemical reactions¹, yet the fleeting configuration when existing chemical bonds dissociate while new ones form is extremely difficult to examine directly². Adiabatic potential-energy surfaces—usually derived using quantum chemical methods³ that assume mutually independent nuclear and electronic motion⁴—quantify the fundamental forces between atoms involved in reaction and thus provide accurate descriptions of a reacting system as it moves through its transition state^{5,6}. This approach, widely tested for gas-phase reactions⁷, is now also commonly applied to chemical reactions at metal surfaces⁸. There is, however, some evidence calling into question the correctness of this theoretical approach for surface reactions: electronic excitation upon highly exothermic chemisorption has been observed⁹, and indirect evidence suggests that large-amplitude vibrations of reactant molecules can excite electrons at metal surfaces^{10,11}. Here we report the detection of ‘hot’ electrons leaving a metal surface as vibrationally highly excited NO molecules collide with it. Electron emission only occurs once the vibrational energy exceeds the surface work function, and is at least 10,000 times more efficient than the emissions seen in similar systems where large-amplitude vibrations were not involved^{12–18}. These observations unambiguously demonstrate the direct conversion of vibrational to electronic excitation, thus questioning one of the basic assumptions currently used in theoretical approaches to describing bond-dissociation at metal surfaces.